Journal of Molecular Liquids 363 (2022) 119843

Contents lists available at ScienceDirect

Journal of Molecular Liquids

journal homepage: www.elsevier.com/locate/molliq

Electrical modification of order parameters and director fluctuations in a dielectrically negative nematic doped with a positive additive

Lu-Yao Sun [a], Xin-Yao Wang [a], Jia-Hao Chen [a], Chao-Yi Li [b,c], Ling-Ling Ma [b,c,*], Yan-Qing Lu [b,c], Bing-Xiang Li [a,b,*]

[a] College of Electronic and Optical Engineering & College of Flexible Electronics (Future Technology), Nanjing University of Posts and Telecommunications, Nanjing 210023, China
[b] National Laboratory of Solid State Microstructures, Nanjing University, Nanjing 210023, China
[c] College of Engineering and Applied Sciences, Nanjing University, Nanjing 210023, China

ARTICLE INFO

Article history:
Received 13 May 2022
Revised 8 July 2022
Accepted 12 July 2022
Available online 16 July 2022

Keywords:
Nematic liquid crystal
Electric field
Order parameter
Dielectric anisotropy
Director fluctuations

ABSTRACT

Electric effects of nematic liquid crystals (NLCs) have enabled the revolution of the display industry. Recently, the electro-optic switching of NLCs has been accelerated by applying electric fields in such a way that the field does not change the director orientation, but modifies the optical tensors of NLCs due to three effects: induced biaxial orientational order, enhanced uniaxial orientational order, and quenching of director fluctuations. Till now, these three effects have been explored only in NLCs with negative dielectric anisotropy. Here, we experimentally study the electrical modification of order parameters and director fluctuations in a dielectrically negative/positive composite NLC. The dielectrically positive dopant causes the following changes: (a) a faster nanosecond switching for optical responses attributed to the change of order parameters, (b) an increase of the biaxial order parameter, (c) a reduction of the uniaxial order parameter, and (d) a slight reduction in the field-induced birefringence change. This work provides a basis for further studies in nanosecond electro-optics.

1. Introduction

Liquid crystals (LCs) have been extensively used in various electro-optic switching devices [1–6] including the well-known LC displays [7–10], owing to their flexible tenability [11–16], stimuli responsiveness [17,18] and adaptive characteristic [19,20]. Nematic LCs (NLCs) is considered as the simplest LCs in which the molecules possess long-range orientation order without positional order. The average orientation of the nematic molecular long axes along a certain direction in space is called the director $\hat{\boldsymbol{n}}$, which is also the optic axis of the material. The orientational order of NLCs brings the dielectric and optic anisotropy, $\Delta\varepsilon = \varepsilon_{\parallel} - \varepsilon_{\perp}$ and $\Delta n = n_e - n_o$, where $\varepsilon_{\parallel}$ and $\varepsilon_{\perp}$ are the dielectric constants measured parallel and perpendicular to $\hat{\boldsymbol{n}}$; n_o and n_e are the ordinary and extraordinary refractive indices, respectively. Traditional electro-optic applications of NLCs are mainly based on the Frederiks effect, where the applied electric field $\boldsymbol{E}$ reorients the $\hat{\boldsymbol{n}}$ [21]. The director of positive NLCs with $\Delta\varepsilon > 0$ realigns along the field, $\hat{\boldsymbol{n}} \| \boldsymbol{E}$, whereas $\hat{\boldsymbol{n}} \perp \boldsymbol{E}$ for the NLCs with $\Delta\varepsilon < 0$. One bottleneck of this type of switching is the slow relaxation of $\hat{\boldsymbol{n}}$ during the field-off process, typically in the order of milliseconds [21–24]. To address this challenge, sustaining effort has been devoted to develop NLCs with optimized anisotropic properties [25], dual-frequency LCs [26,27], or ferroelectric LCs [28] to speed up the responses ranging from hundreds of microseconds to several microseconds.

Recently, nanosecond electric modification of order parameter (NEMOP) effect was newly proposed by V. Borshch et al. [29]. The electric field changes the order parameters (OPs) of NLCs, including the induced biaxial order and enhanced uniaxial order (rather than altering the director orientations), which leads to fast switching-on and switching-off electro-optic responses in the time scale of nanoseconds [29–31]. For example, Li et al experimentally demonstrated a larger field-induced birefringence change δn in NLCs with the response time reduced to tens of nanoseconds [31]. Despite undisputable finding, previous studies on the NEMOP effect mainly focused on the dielectrically negative NLCs. It is still an open question how a negative/positive composite NLC (a small amount of additive with $\Delta\varepsilon > 0$ doped into a negative NLC) behaves under the perpendicular electric field, including modifications of OPs as well as the field-induced quenching of the director fluctuations.

In this work, we experimentally explore the fast electro-optic response of the dielectrically negative nematic doped with a

* Corresponding authors.
E-mail addresses: malingling@nju.edu.cn (L.-L. Ma), bxli@njupt.edu.cn (B.-X. Li).

https://doi.org/10.1016/j.molliq.2022.119843
0167-7322/

positive additive by applying the electric field perpendicular to the $\hat{\boldsymbol{n}}$ in two experimental geometries. The modifications of the orientational order and director fluctuations of such negative/positive composite NLC are demonstrated by comparing to those of the negative nematic host ($\Delta\varepsilon < 0$). The numerical simulations show that the modifications of OPs and the director fluctuations have different contributions to the field-induced birefringence change. Both uniaxial and biaxial contributions are quadratic with the applied electric field, and the contribution of the director fluctuations quenching is somehow linear to the field. The total switching-on and switching-off time of modifying biaxial and uniaxial OPs are on the order of nanoseconds and become even faster after doped with the positive NLC.

2. Experimental materials and methods

We use two NLCs MLC2080 ($\Delta\varepsilon = -6.4$ @1 kHz, $\Delta n = 0.11$ @589 nm) and MLC2144 ($\Delta\varepsilon = +47$ @ 1 kHz, $\Delta n = 0.25$ @589 nm) both from Merck. To study the effect of doping material with $\Delta\varepsilon > 0$, we prepare a mixture MLC2080&2144 ($\Delta\varepsilon = -1.85$ @ 1 kHz, $\Delta n = 0.12$ @589 nm, 23°C) composed of 88 wt.% MLC2080 and 12 wt.% MLC2144. For convenience, we call these two materials as M2080 and M2080&2144 for short, respectively. To prepare M2080&2144, two NLC materials MLC2080 and MLC2144 are dissolved in chloroform, vibrated with a vortex shaker at a speed of 1500 r/min for 10 min, and then stirred in an ultrasonic bath for 75 min at 45°C, followed by evaporation of chloroform in the vacuum oven 12 h at room temperature and 12 h at 60°C. The NLCs are injected into cells in the isotropic phase. The cells are comprised of two glass plates with transparent electrodes (indium tin oxide, ITO) of low resistivity (10 Ω/sq). Silica spheres of diameter $d = 4.5$ μm are used to separate the two parallel glass plates. Unidirectionally rubbing polyimide PI-2555 (HD MicroSystems) coated on the inner surfaces of two plates provides the NLCs a parallel alignment. To study the electric-optic response of M2080 and M2080&2144, the He-Ne laser beam of wavelength $\lambda = 632.8$ nm passes through a polarizer, the NLC cell, Soleil-Babinet compensator (THORLABS), and the other polarizer crossed with the first one. The linearly polarized laser beam enters the NLC cells at the angle of 45°. The transmitted light intensity is measured by a photodetector DET025AL/M (THORLABS, response time < 1 ns). A voltage pulse of duration 400 ns is applied by a pulse generator HV 1000 (Director Energy) with sharp rise and fall edges of characteristic time 1 ns. The applied voltage pulses and photodetector signals are recorded with 1 G sample/s digital oscilloscope DS1202 (RIGOL).

To explore the electro-optic contributions $\delta\tilde{\varepsilon}_u$, $\delta\tilde{\varepsilon}_b$, and $\delta\tilde{\varepsilon}_f$ which are from the enhanced uniaxial OP, the induced biaxial OP, and the quenching of the director fluctuations, respectively, we perform electro-optic experiments in two geometries: (1) "Biaxial-uniaxial" (BU) geometry in which only the biaxial and uniaxial OPs contribute to the δn, and the contribution from the quenching of the director fluctuations is zero. In this case, a linearly polarized laser beam propagates inside the nematic slab at an angle of 45° with respect to the cell normal, Fig. 1(a). The director $\hat{\boldsymbol{n}}$ orients parallelly to the plane of incidence. The field-induced effective birefringence change δn_{BU} in geometry BU is expressed as [30]:

$$\delta n_{\mathrm{BU}} = \frac{n_o/n_e + 1 + n_e/n_o}{6\sqrt{n_e^2 - n_o^2}}\left(\delta\tilde{\varepsilon}_u + \frac{3}{2}\delta\tilde{\varepsilon}_b\right) \tag{1}$$

$$\delta\tilde{\varepsilon}_j(t) = \frac{\alpha_j}{\tau_j}\int_0^t E^2(t')\exp[(t'-t)/\tau_j]dt' \tag{2}$$

where j reads u or b depending on the nature of contribution, τ_u and τ_b are the uniaxial and biaxial relaxation times, and α_u and α_b are the effective uniaxial and biaxial susceptibilities, respectively. $E(t)$ represents the electric field applied. (2) "Uniaxial-fluctuations" (UF) geometry: the contribution of the biaxial OP is eliminated, and only the changes in the uniaxial OP and the director quenching contribute to the modification of the optical tensor. In this case, the director $\hat{\boldsymbol{n}}$ orients perpendicularly to the plane of incidence, Fig. 1 (b). The field-induced effective birefringence change δn_{UF} in geometry UF is expressed as [30]:

$$\delta n_{\mathrm{UF}} = \frac{1}{3\sqrt{2}}\left(\frac{1}{n_o} + \frac{2}{\sqrt{2n_e^2 - n_o^2}}\right)\left(\delta\tilde{\varepsilon}_u + \frac{3}{2}\delta\tilde{\varepsilon}_f\right) \tag{3}$$

$$\delta\tilde{\varepsilon}_f(t) = A\frac{e^{-S(t)}}{\sqrt{\gamma_{\mathrm{eff}}}}\int_0^t \frac{f_E(t')}{\sqrt{(t-t')}}\, e^{S(t')}dt' \tag{4}$$

where $S(t) = \frac{1}{\gamma_{\mathrm{eff}}}\int_0^t f_E(t')dt'$ and $f_E(t) = \varepsilon_0|\Delta\varepsilon|\left[\int_t^\infty \frac{e^{-t'}}{t'}dt'\right]^2$. The coefficient A and the effective rotational viscosity γ_{eff} of NLCs are the fitting parameters, and $\varepsilon_0 = 8.85\times10^{-12}$ F/m is the dielectric constant in vacuum.

The δn can be calculated from the dynamics of the transmitted light intensity as [32]:

$$\delta n = \frac{\lambda}{\pi L}\left\{-\frac{1}{2}\arccos\Delta I(t) - \arccos[1 - 2I_{\mathrm{A}}(t)]\right\} \tag{5}$$

where $\Delta I(t) = 1 - I_{\mathrm{A}}(t) - I_{\mathrm{A}}(0) - I_{\mathrm{B}}(t) + I_{\mathrm{B}}(0)$. $I_{\mathrm{A}}(0) = I_{\mathrm{B}}(0)$ are the transmitted light intensity measured at the field-free initial state, as shown in Fig. 1(c), (d). To eliminate the parasitic effects on the δn, we measure the dynamics of the light intensity $I_{\mathrm{A}}(t)$ and $I_{\mathrm{B}}(t)$ with two compensator settings ϕ_{A} and ϕ_{B}, respectively, where the phase retardance difference is $|\phi_{\mathrm{B}} - \phi_{\mathrm{A}}| < \pi$.

3. Experimental results and simulations

3.1. Electro-optic responses of NLCs in geometries BU and UF

To obtain electro-optic responses of the NLCs contributed from the modification of the biaxial and uniaxial order parameters, 400 ns-duration voltage pulses are applied onto the NLC cells of thickness $d = 4.5$ μm in geometry BU. In geometry BU, the δn of two materials are positive and increase with the growth of the applied electric field, Fig. 2(a), (b). The maximum field-induced birefringence change δn_{max} of M2080&2144 does not decrease much, about 10% reduction compared with that of M2080 at all the applied electric fields, Fig. 2(c). The δn_{max} shows a quadratic dependence on the electric field for both M2080 and M2080&2144, Fig. 2(d).

To investigate the optic contributions from the uniaxial order change and the quenching of the director fluctuations, we perform the electro-optic experiments in geometry UF. In this geometry, δn is positive for M2080, Fig. 3(a). With the MLC2144 doped, δn of M2080&2144 is negative first, and then becomes positive gradually, Fig. 3(b). At the moment when the electric field is removed, the δn increases rapidly and then decreases slowly. The δn_{max} of M2080&2144 is smaller than that of M2080 during the pulse duration, Fig. 3(c). Compared with M2080, δn_{max} of M2080&2144 decreases by about 50% for all electric fields, Fig. 3(c). As the applied electric field increasing, the maximum field-induced birefringence change δn_{max} is also getting larger for two materials, Fig. 3(d). The δn_{max} linearly grows with the electric field for these two materials in geometry UF.

Electro-optic switching speed of NLCs is one of the critical factors for the practical applications. To characterize it, we use the industry-standard 10–90 technique [32] to calculate the

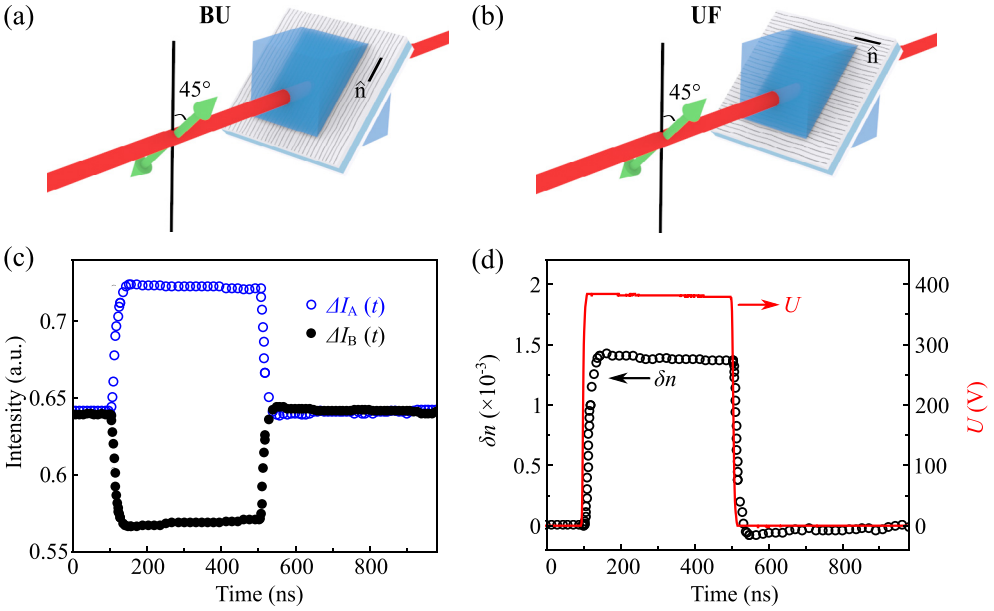

Fig. 1. Optical geometries and responses. (a) Geometry BU: $\hat{\boldsymbol{n}}$ orients parallel to the plane of incidence. (b) Geometry UF: $\hat{\boldsymbol{n}}$ is normal to the plane of incidence. Two black short lines represent the alignment of NLCs. Green bidirectional arrows indicate the incident polarizations. In two geometries, the polarization of the incident light is 45° relative to the plane of incidence, in which the incident angles are both 45°. Dynamics of (c) the transmitted light intensity of M2080 and (d) the corresponding field-induced birefringence change δn in response to the applied voltage pulse $U_0 = 382\,\mathrm{V}$ in geometry BU.

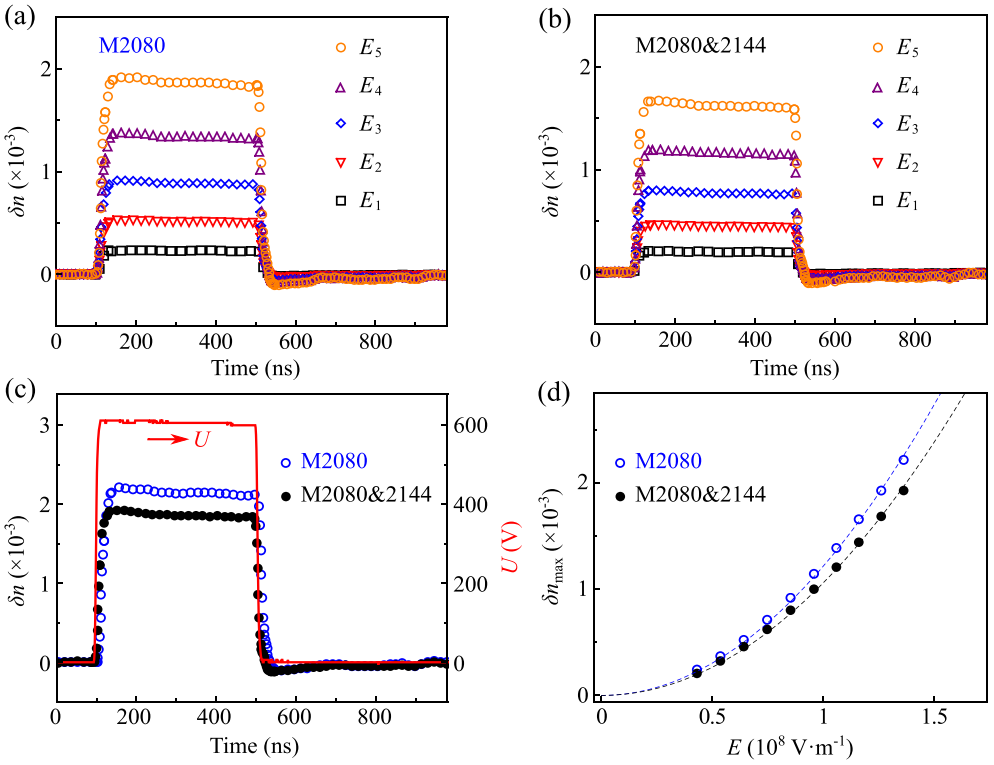

Fig. 2. Electro-optic responses of M2080 and M2080&2144 in geometry BU. Dynamics of field-induced birefringence change for (a) M2080 and (b) M2080&2144 to electric fields of amplitude $E_1 = 0.4 \times 10^8\,\mathrm{V\cdot m^{-1}}$, $E_2 = 0.6 \times 10^8\,\mathrm{V\cdot m^{-1}}$, $E_3 = 0.8 \times 10^8\,\mathrm{V\cdot m^{-1}}$, $E_4 = 1.0 \times 10^8\,\mathrm{V\cdot m^{-1}}$, $E_5 = 1.3 \times 10^8\,\mathrm{V\cdot m^{-1}}$, respectively. (c) Dynamics of field-induced birefringence change in response to an amplitude of electric field $E = 1.4 \times 10^8\,\mathrm{V\cdot m^{-1}}$. (d) Dependences of the maximum of field-induced birefringence change on the applied electric field. The dashed lines represent the parabola fitting $\delta n_{\max} = \alpha E^2$ with the coefficients $\alpha \approx 1.2 \times 10^{-19}\,\mathrm{V^{-2}\cdot m^2}$ for M2080 and $\alpha \approx 1.0 \times 10^{-19}\,\mathrm{V^{-2}\cdot m^2}$ for M20802144. The working temperature is 23°C.

switching-on and switching-off times of the electro-optic responses in two geometries. Interestingly, in geometry BU, the doped MLC2144 speeds up the field-on and field-off processes of M2080, Fig. 4(a), (b). The average switching times $\bar{\tau}_{on}$ and $\bar{\tau}_{off}$ of M2080&2144 are about 20% and 15% faster than that of M2080, respectively. In geometry UF, $\bar{\tau}_{on}$ and $\bar{\tau}_{off}$ are on the order of sub-microsecond, which is one order of magnitude larger than that in geometry BU, Fig. 4(c), (d). The switching-off time of

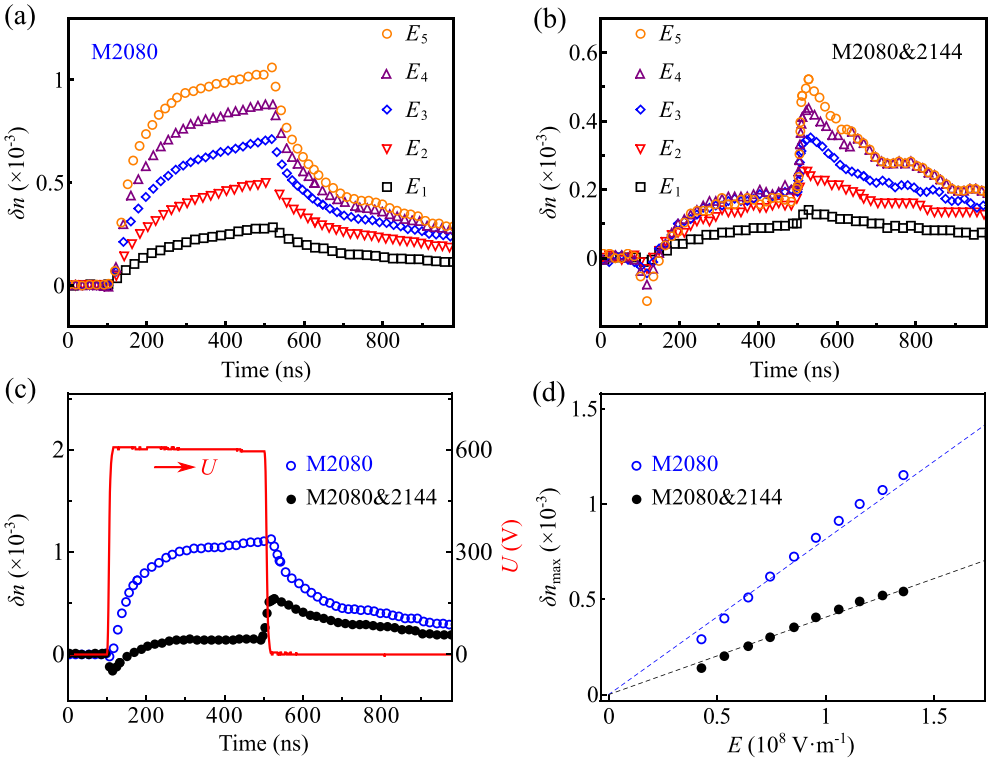

Fig. 3. Electro-optic responses of M2080 and M2080&2144 in geometry UF. Dynamics of field-induced birefringence change for (a) M2080 and (b) M2080&2144 to electric fields of amplitude $E_1 = 0.4 \times 10^8 \mathrm{V \cdot m^{-1}}$, $E_2 = 0.6 \times 10^8 \mathrm{V \cdot m^{-1}}$, $E_3 = 0.8 \times 10^8 \mathrm{V \cdot m^{-1}}$, $E_4 = 1.0 \times 10^8 \mathrm{V \cdot m^{-1}}$, $E_5 = 1.3 \times 10^8 \mathrm{V \cdot m^{-1}}$, respectively. (c) Dynamics of field-induced birefringence change in response to an electric pulse of amplitude $E = 1.4 \times 10^8 \mathrm{V \cdot m^{-1}}$. (d) Dependences of the field-induced birefringence change on the applied electric field. The dashed lines show the linear fitting $\delta n_{\max} = \beta E$ with the coefficients $\beta \approx 0.8 \times 10^{-19}\ \mathrm{V^{-1} \cdot m}$ and $\beta \approx 0.4 \times 10^{-19}\ \mathrm{V^{-1} \cdot m}$ for M2080 and M2080&2144, respectively. The working temperature is 23°C.

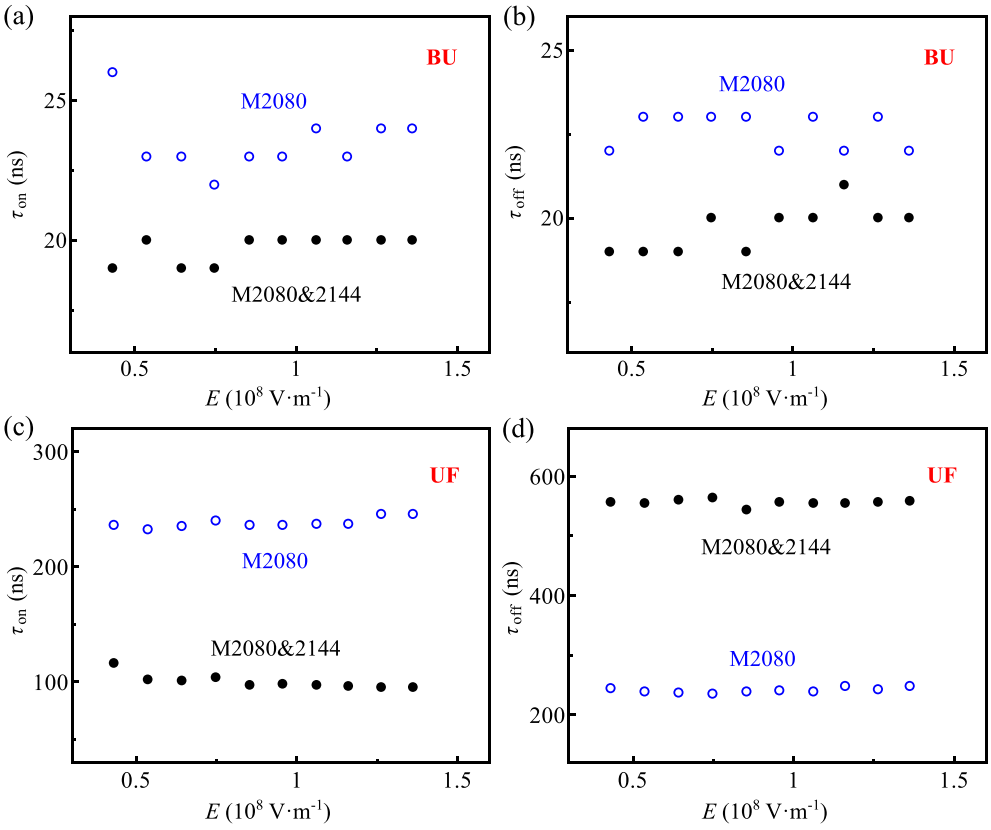

Fig.4. Characteristic times of the NLCs M2080 and M2080&2144. (a) τ_{on} and (b) τ_{off} as a function of the applied electric fields in geometry BU. Electric dependences of (c) τ_{on} and (d) τ_{off} in geometry UF. The working temperature is 23°C.

M2080&2144 is shorter than that of M2080, but the switching-on process of M2080&2144 is slower than that of M2080.

3.2. Numerical simulations of contributions from three electric mechanisms

To separate the optical contributions from the changes of the biaxial and uniaxial order parameters, we fit the electro-optic responses of M2080 and M2080&2144 measured in geometry BU, using Eqs. (1) and (2). As shown in Fig. 5(a), (b), both contributions from the changes of the uniaxial and biaxial OPs to δn are positive, while for the NLC M2080&2144, the induced biaxial order parameter still increases the birefringence of NLC from about 1.7×10^{-3} to 2.2×10^{-3}, showing a positive contribution to δn. But the uniaxial order parameter exhibits a negative contribution (the δn coming from the uniaxial OP changes decreases from 0.3×10^{-3} to -0.4×10^{-3}), which indicates a reduction of the uniaxial order parameter of the material.

To figure out the optical response contributed from the quenching of the director fluctuations, we fit the dynamics of δn of the NLCs M2080 and M2080&2144 in geometry UF with Eqs. (3) and (4). As shown in Fig. 6(a), (b), in geometry UF, two contributions from the change of the uniaxial OP and the quenching of the director fluctuations are positive for the NLC M2080. For M2080&2144, the contribution of the director fluctuations quenching is positive and causes an increase of the birefringence of NLC. The uniaxial OP brings a negative contribution on the δn and somehow decreases the birefringence of M2080&2144, which is identical to what we have obtained from the fitting in geometry BU.

Now, we can explore the field dependence of the δn from the fitting of biaxial, uniaxial contributions in geometry BU and the contribution of the director fluctuations quenching in geometry UF. For two different materials, with the increase of the applied electric field, the absolute value of the three mechanisms' contributions increases, Fig. 7(a), (b). The results further suggest that, (a) $\delta n \propto E^2$ for both contributions from the modifications of the biaxial and uniaxial order parameters and (b) $\delta n \propto E$ for contribution from the quenching of the director fluctuations. Here, we fit the contributions from biaxial and uniaxial OPs with $\delta n_{b,u} = u_{b,u}E^2$, and the contribution of the director fluctuations quenching with $\delta n_f = \nu_f E$. The fitting results show an increase of the biaxial coefficient u_b from 9.6×10^{-20} V$^{-2}\cdot$m^2 to 1.23×10^{-19} V$^{-2}\cdot$m^2, a sign reversal of the uniaxial coefficient u_u from positive to negative, and no changes in the fluctuation term, which further indicate the enhanced induction of biaxiality, the reduced uniaxiality, and unchanged quenching of director fluctuations.

The enhanced induction of biaxial order parameter and the reduction of the uniaxial order parameter could be explained from a microscopic point of view. We assume that the dipole in the molecules of the NLC M2080 ($\Delta\varepsilon < 0$) is perpendicular to the

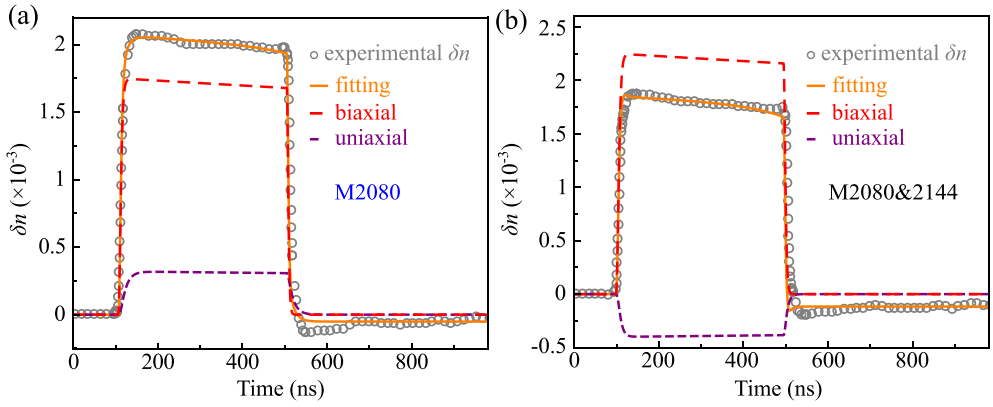

Fig. 5. Experimental result and fitting of optic responses measured in geometry BU at $E = 1.4 \times 10^8$V$\cdot$m^{-1}. According to Eq. (2), the fitting parameters are (a) $\tau_u \approx 12$ ns, $\tau_b \approx 1$ ns, $\alpha_u \approx 0.32 \times 10^{-20}$ m$^2\cdot$V^{-2}, and $\alpha_b \approx 1.75 \times 10^{-20}$ m$^2\cdot$V^{-2} for M2080, and (b) $\tau_u \approx 6$ ns, $\tau_b \approx 2$ ns, $\alpha_u \approx -0.4 \times 10^{-20}$ m$^2\cdot$V^{-2}, and $\alpha_b \approx 2.25 \times 10^{-20}$ m$^2\cdot$V^{-2} for M2080&2144. The grey circles represent the experimental birefringence change δn and the orange solid line is the fitted δn. The dashed lines show the fitting of δn from the changes of biaxial (red) and uniaxial (purple) order parameters, respectively. The working temperature is 23°C.

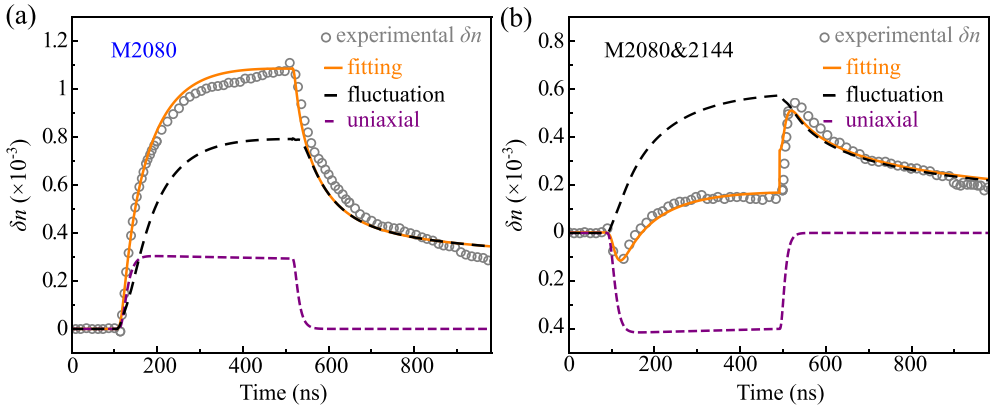

Fig. 6. Experimental results and fitting of optic response measured in geometry UF at $E = 1.4 \times 10^8$V$\cdot$m^{-1} fitted with Eqs. (2) and (4). (a) $\tau_u \approx 12$ ns, $\alpha_u \approx 0.32 \times 10^{-20}$ m$^2\cdot$V^{-2}, $A \approx 7$ μs$\cdot$(m/kg)$^{1/2}$ and $\gamma_{\text{eff}} \approx 88$ mPa$\cdot$s for M2080 and (b) $\tau_u \approx 6$ ns, $\alpha_u \approx -0.4 \times 10^{-20}$ m$^2\cdot$V^{-2}, $A \approx 20$ μs$\cdot$(m/kg)$^{1/2}$ and $\gamma_{\text{eff}} \approx 60$ mPa$\cdot$s for M2080&2144, respectively. The grey circles represent the experimental birefringence change δn and the orange solid line is the fitted δn. The dashed lines show the fitting of δn from the quenching of the director fluctuations (black) and the change of the uniaxial (purple) order parameter, respectively. The working temperature is 23°C.

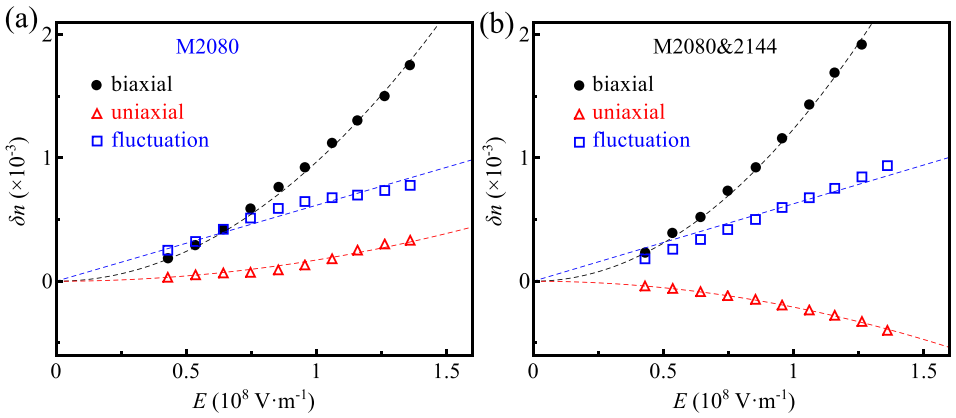

Fig. 7. Dependences of the field-induced birefringence change contributed from three mechanisms for M2080 (a) and M2080&2144 (b) with $\delta n_{b,u} = u_{b,u}E^2$ and $\delta n_f = v_f E$. The fitting coefficients for M2080 in (a) are $u_b \approx 9.6 \times 10^{-20}$ V$^{-2}\cdot$m^2, $u_u \approx 1.7 \times 10^{-20}$ V$^{-2}\cdot$m^2, and $v_f \approx 6.2 \times 10^{-12}$ V$^{-1}\cdot$m. The coefficients for M2080&2144 in (b) are $u_b \approx 1.23 \times 10^{-19}$ V$^{-2}\cdot$m^2, $u_u \approx -2.1 \times 10^{-20}$ V$^{-2}\cdot$m^2, and $v_f \approx 6.3 \times 10^{-12}$ V$^{-1}\cdot$m. The black and red lines are the parabola fitted curves. The blue dashed line is the linear fitting.

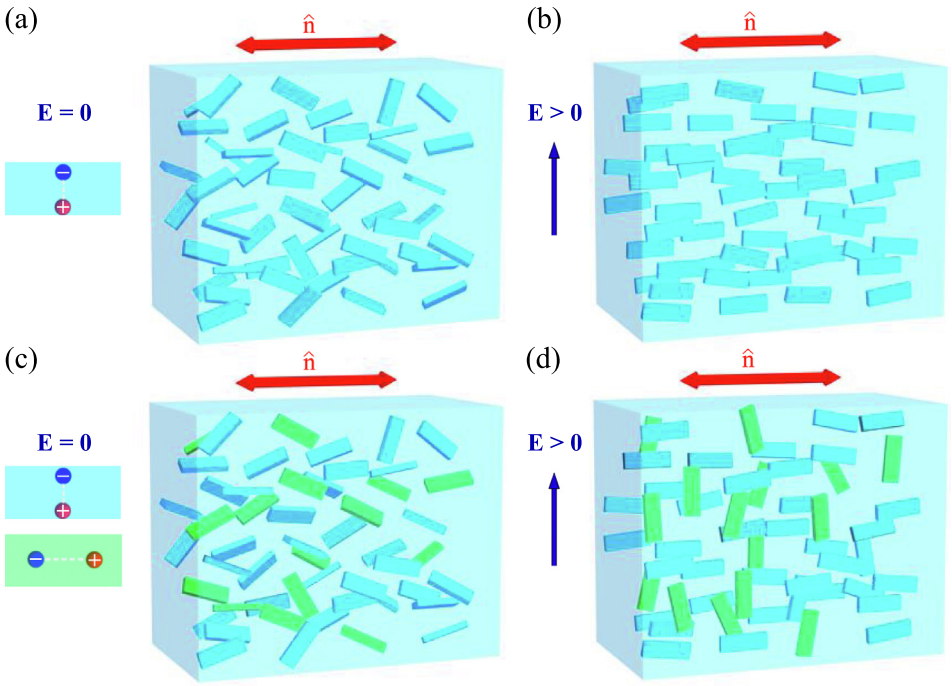

Fig. 8. Schematic illustration of the field-modified-order-parameter effect for two nematic systems. Orientational order of LC (e.g. M2080) molecules with transverse dipole in (a) the absence and (b) the existence of an electric field. Orientational order of LC (e.g. M2080&2144) two types of molecules with transverse and longitudinal dipoles in (c) the absence and (d) the presence of an electric field. The cuboids represent molecules of NLC MLC2080 (cyan) and MLC2144 (green), respectively, in which the positive (red sphere) and negative (blue sphere) electric charges indicate the direction of dipoles. The arrows show the director $\hat{\boldsymbol{n}}$ (red double arrows) and the applied field (blue arrows).

molecular long axis for the simplicity, Fig. 8(a). When an electric field perpendicular to the director $\hat{\boldsymbol{n}}$ is applied, the molecules of M2080 prefer to align perpendicularly to the field and parallelly to the director, which enhances the uniaxial OP, Fig. 8(b). We further assume that the dipole of MLC2144 ($\Delta\varepsilon > 0$) parallels to the molecular long axis. As shown in Fig. 8(c), the mixed nematic system has both molecules with transverse and longitudinal dipoles, where the cyan and green cuboids represent the molecules of M2080 and MLC2144, respectively. The NLC molecules possess a uniaxial orientational order in the field-free state, Fig. 8(c). After the electric field applied perpendicularly to the director, the molecules with transverse dipole are more likely aligned parallel to the $\hat{\boldsymbol{n}}$, while the molecules with longitudinal dipole prefer to align perpendicular to the $\hat{\boldsymbol{n}}$, Fig. 8(d), which causes a reduction of the uniaxial OP. This is why the electro-optic contribution of the uniaxial order parameter change of M2080&2144 is negative.

4. Discussions and conclusions

We experimentally compare the electro-optic responses of two NLCs, which are the dielectrically negative NLC M2080 and the mixture M2080&2144 composed of both dielectrically positive and negative components. For the NLC M2080 ($\Delta\varepsilon \approx -6.4$), the experimental results in both geometries BU and UF show that the applied field causes the increase of the effective birefringence Δn_{eff} of the NLC, and the theoretical fitting suggests that the field induces the biaxial order parameter, enhances the uniaxial order parameter and quenches the director fluctuations. Consequently,

all the three mechanisms provide positive contributions to the fast response. The maximum field-induced effective birefringence change shows a quadratic dependence on the electric field in geometry BU and a linear dependence on E in geometry UF. The response times of M2080 are tens of nanoseconds in geometry BU and hundreds of nanoseconds in geometry UF. For the mixture M2080&2144 with $\Delta\varepsilon \approx -1.8$, it exhibits the same electric dependence of the $\delta n_{\max}$ and faster responses for the switching-on and switching-off processes in geometry BU, compared with M2080. Although the $\Delta\varepsilon$ of NLC decreases 60%, the field-induced birefringence reduces by about 10% at all electric fields in geometry BU. This is somehow unexpected in Ref. [31], which has demonstrated lower dielectric anisotropy would exhibit much smaller field-induced birefringence change in the nematic systems comprised of rod-like molecules with transverse dipole. The reason of the slight change in the field induced birefringence δn in geometry BU is that the main contribution coming from the induced biaxiality rather than from the enhanced uniaxial order. The fitting results suggest that the field further enhances the induced biaxiality and reduces the uniaxial order of the mixture M2080&2144. For both materials M2080 and M2080&2144, the optical contributions from the biaxial and uniaxial orders are proportional to E^2, while the contribution from the quenching of the director fluctuations is proportional to E, which is consistent with Ref. [12,30]. To describe the biaxiality of a LC system, one can use the typical parameter β in the range from 0 to 1, i.e. $\beta = 0$ represents a uniaxial state, $\beta = 1$ indicates the maximum biaxiality, where $\beta^2 = 1 - 6(\mathrm{tr}\mathbf{Q}^3)^2/(\mathrm{tr}\mathbf{Q}^2)^3$ and $\mathbf{Q}$ is a tensor of order parameter [33]. For the simplicity, we use a diagonal tensor with three nonzero components $(-S/3, -S/3, 2S/3)$ for the uniaxial NLC at the field free state, where S is the nematic order parameter. Taking the field-free birefringence $\Delta n \propto S$ [15] and the field-induced birefringence change δn_u, δn_b, we naively assume the field induced changes of the biaxial and uniaxial order parameters are $\Delta S_b = S\delta n_b/\Delta n$ and $\Delta S_u = S\delta n_u/\Delta n$, respectively. Therefore, $(-S/3 + \Delta S_b - \Delta S_u, -S/3 - \Delta S_b - \Delta S_u, 2S/3 + 2\Delta S_u)$. At $E = 1.4 \times 10^8\,\mathrm{V\cdot m^{-1}}$, $\delta n_u \approx 0.33 \times 10^{-3}$, $\delta n_b \approx 1.75 \times 10^{-3}$ for M2080 and $\delta n_u \approx -0.4 \times 10^{-3}$, $\delta n_b \approx 2.25 \times 10^{-3}$ for M2080&2144, which lead to the values of β, 0.08 for M2080 and 0.10 for M2080&2144. The explored system can extend the understanding of the fast electric-optic response by modifying the order parameters and quenching the LC fluctuations, and provide inspirations in further improvement of the switching time, which may enable ultrafast polarization-tailored optical devices.

CRediT authorship contribution statement

Lu-Yao Sun: Software, Investigation, Data curation. **Xin-Yao Wang:** Investigation, Methodology. **Jia-Hao Chen:** Data curation, Visualization. **Chao-Yi Li:** Data curation, Validation. **Ling-Ling Ma:** Visualization, Writing – review & editing, Funding Acquisition. **Yan-Qing Lu:** Writing – review & editing, Funding Acquisition. **Bing-Xiang Li:** Conceptualization, Supervision, Writing – original draft, Writing – review & editing, Funding Acquisition.

Data availability

Data will be made available on request.

Declaration of Competing Interest

The authors declare that they have no known competing financial interests or personal relationships that could have appeared to influence the work reported in this paper.

Acknowledgements

Funding: This work was supported by the National Key Research and Development Program of China (No. 2021YFA1202000), the National Natural Science Foundation of China (Nos. 52003115, RK106LH21001) and Natural Science Foundation of Jiangsu Province (Nos. BK20212004 and BK20200320). The authors gratefully appreciate Prof. Oleg D. Lavrentovich, Dr. S. V. Shiyanovskii, and Dr. V. Borshch for their constructive discussions.

References

[1] Shuaijia Huang, Yan Li, Pengcheng Zhou, Shuxin Liu, Yikai Su, Polymer network liquid crystal grating/fresnel lens fabricated by holography, Liq. Cryst. 44 (5) (2017) 873–879, https://doi.org/10.1080/02678292.2016.1254295.
[2] Haitao Dai, Lin Chen, Bin Zhang, Guangyuan Si, Yan Jun Liu, Optically isotropic, electrically tunable liquid crystal droplet arrays formed by photopolymerization-induced phase separation, Opt. Lett. 40 (12) (2015) 2723, https://doi.org/10.1364/OL.40.002723.
[3] P. Chen, Y.-Q. Lu, W. Hu, et al., Beam shaping via photopatterned liquid crystals, Liq. Cryst. 43 (2016) 2051–2061, https://doi.org/10.1080/02678292.2016.1191685.
[4] Seyed Reza Seyednejad, Mohammad Reza Mozaffari, Conically degenerate anchoring effect in planar nematic-liquid-crystal shells, Phys. Rev. E 104 (1) (2021), https://doi.org/10.1103/PhysRevE.104.014701.
[5] Ziqian He, Kun Yin, Shin-Tson Wu, Miniature planar telescopes for efficient, wide-angle, high-precision beam steering, Light Sci. Appl. 10 (1) (2021), https://doi.org/10.1038/s41377-021-00576-9.
[6] Lingling Ma, Chaoyi Li, Luyao Sun, Zhenpeng Song, Yanqing Lu, Bingxiang Li, Submicrosecond electro-optical switching of one-dimensional soft photonic crystals, Photonics Res. 10 (3) (2022) 786, https://doi.org/10.1364/prj.449284.
[7] Xiao Li, Chao Ping Chen, Yan Li, Pengcheng Zhou, Xinhong Jiang, Na Rong, Shuxin Liu, Gufeng He, Jiangang Lu, Yikai Su, High-efficiency video-rate holographic display using quantum dot doped liquid crystal, J. Display Technol. 12 (4) (2016) 362–367, https://doi.org/10.1109/JDT.2015.2491965.
[8] Yuan Shen, Yan-Chao Xu, Ya-Hao Ge, Rong-guo Jiang, Xiao-Zhong Wang, Sen-Sen Li, Lu-Jian Chen, Photoalignment of dye-doped cholesteric liquid crystals for electrically tunable patterns with fingerprint textures, Opt. Express 26 (2) (2018) 1422, https://doi.org/10.1364/OE.26.001422.
[9] Hai-Wei Chen, Jiun-Haw Lee, Bo-Yen Lin, Stanley Chen, Shin-Tson Wu, Liquid crystal display and organic light-emitting diode display: Present status and future perspectives, Light Sci. Appl. 7 (3) (2018) 17168, https://doi.org/10.1038/lsa.2017.168.
[10] Govind Pathak, Gurumurthy Hegde, Veena Prasad, Investigation of electro-optical and dielectric properties of nematic liquid crystal dispersed with biowaste based porous carbon nanoparticles: Increased birefringence for display applications, J. Mol. Liq. 314 (2020) 113643, https://doi.org/10.1016/j.molliq.2020.113643.
[11] Chenhui Peng, Oleg Lavrentovich, Liquid Crystals-Enabled AC Electrokinetics, Micromachines 10 (1) (2019) 45, https://doi.org/10.3390/mi10010045.
[12] Oleg D. Lavrentovich, Israel Lazo, Oleg P. Pishnyak, Nonlinear electrophoresis of dielectric and metal spheres in a nematic liquid crystal, Nature 467 (7318) (2010) 947–950, https://doi.org/10.1038/nature09427.
[13] Bing-Xiang Li, Rui-Lin Xiao, Sathyanarayana Paladugu, Sergij V. Shiyanovskii, Oleg D. Lavrentovich, Three-dimensional solitary waves with electrically tunable direction of propagation in nematics, Nat. Commun. 10 (1) (2019), https://doi.org/10.1038/s41467-019-11768-8.
[14] Bing-Xiang Li, Volodymyr Borshch, Rui-Lin Xiao, Sathyanarayana Paladugu, Taras Turiv, Sergij V. Shiyanovskii, Oleg D. Lavrentovich, Electrically driven three-dimensional solitary waves as director bullets in nematic liquid crystals, Nat. Commun. 9 (1) (2018), https://doi.org/10.1038/s41467-018-05101-y.
[15] D.-K. Yang, S.-T. Wu, Fundamentals of liquid crystal devices, John Wiley & Sons, Ltd, Chichester, 2006.
[16] P.G. De Gennes, J. Prost, The physics of liquid crystals, Oxford University Press, Oxford, 1995.
[17] Hu Dou, Fan Chu, Yu-Qiang Guo, Li-Lan Tian, Qiong-Hua Wang, Yu-Bao Sun, Large aperture liquid crystal lens array using a composited alignment layer, Opt. Express 26 (7) (2018) 9254, https://doi.org/10.1364/OE.26.009254.
[18] Ahmad M. Labeeb, Yassmin A. Ward, Mohamed Fikry, Thermal control of tunable photonic optical bandgaps in different cholesteric liquid crystals mixtures, J. Mol. Liq. 340 (2021) 117179, https://doi.org/10.1016/j.molliq.2021.117179.
[19] Ling Wang, Hari Krishna Bisoyi, Zhigang Zheng, Karla G. Gutierrez-Cuevas, Gautam Singh, Satyendra Kumar, Timothy J. Bunning, Quan Li, Stimuli-directed self-organized chiral superstructures for adaptive windows enabled by mesogen-functionalized graphene, Mater. Today 20 (5) (2017) 230–237, https://doi.org/10.1016/j.mattod.2017.04.028.
[20] Hari Krishna Bisoyi, Quan Li, Liquid crystals: Versatile self-organized smart soft materials, Chem. Rev. 122 (5) (2022) 4887–4926, https://doi.org/10.1021/acs.chemrev.1c00761.

[21] L.M. Blinov, V.G. Chigrinov, J.S. Patel, Electrooptic Effects in Liquid Crystal Materials, Springer, New York, 1995.
[22] Hossein Nemati, Shiyi Liu, Rafael S. Zola, Vincent P. Tondiglia, Kyung Min Lee, Timothy White, Timothy Bunning, Deng-Ke Yang, Mechanism of electrically induced photonic band gap broadening in polymer stabilized cholesteric liquid crystals with negative dielectric anisotropies, Soft Matter 11 (6) (2015) 1208–1213, https://doi.org/10.1039/C4SM02283A.
[23] Kyung Min Lee, Ecklin P. Crenshaw, Mariacristina Rumi, Timothy J. White, Timothy J. Bunning, Michael E. McConney, Effect of Cell Thickness on the Electro-optic Response of Polymer Stabilized Cholesteric Liquid Crystals with Negative Dielectric Anisotropy, Materials 13 (3) (2020) 746, https://doi.org/10.3390/ma13030746.
[24] Hitesh Khandelwal, Michael G. Debije, Timothy J. White, Albertus P.H.J. Schenning, Electrically tunable infrared reflector with adjustable bandwidth broadening up to 1100 nm, J. Mater. Chem. A 4 (16) (2016) 6064–6069, https://doi.org/10.1039/C6TA01647B.
[25] Yi-Hsin Lin, Yu-Jen Wang, Hung-Chun Lin, Ming-Long Lee, Po-Lun Chen, Optical measurement in a curved optical medium with optical birefringence and anisotropic absorption, Opt. Express 29 (23) (2021) 38654, https://doi.org/10.1364/OE.439521.
[26] Bing-Xiang Li, Rui-Lin Xiao, Sathyanarayana Paladugu, Sergij V. Shiyanovskii, Oleg D. Lavrentovich, Dye-doped dual-frequency nematic cells as fast-switching polarization-independent shutters, Opt. Express 27 (4) (2019) 3861, https://doi.org/10.1364/OE.27.003861.
[27] Chun-Yen Liu, Chi-Feng Yen, Yi-Hua Hung, Chia-Min Tu, Guan-Yi Wu, Hung-Yi Chen, Polymer-stabilized bistable dual-frequency cholesteric liquid crystal devices assisted by a predesigned chiral dopant, J. Mater. Sci. Lett. 9 (46) (2021) 16672–16681, https://doi.org/10.1039/D1TC04354D.
[28] Wang Hu, Haiyan Zhao, Li Song, Zhou Yang, Hui Cao, Zihui Cheng, Qing Liu, Huai Yang, Electrically controllable selective reflection of chiral nematic liquid crystal/chiral ionic liquid composites, Adv. Mater. 22 (4) (2010) 468–472, https://doi.org/10.1002/adma.200902213.
[29] V. Borshch, S.V. Shiyanovskii, O.D. Lavrentovich, et al., Nanosecond electro-optic switching of a liquid crystal, Phys. Rev. Lett. 111 (2013) 107802, https://doi.org/10.1103/PhysRevLett.111.107802.
[30] Volodymyr Borshch, Sergij V. Shiyanovskii, Bing-Xiang Li, Oleg D. Lavrentovich, Nanosecond electro-optics of a nematic liquid crystal with negative dielectric anisotropy, Phys. Rev. E 90 (6) (2014) 062504, https://doi.org/10.1103/PhysRevE.90.062504.
[31] Bing-Xiang Li, Volodymyr Borshch, Sergij V. Shiyanovskii, Shao-Bin Liu, Oleg D. Lavrentovich, Electro-optic switching of dielectrically negative nematic through nanosecond electric modification of order parameter, Appl. Phys. Lett. 104 (20) (2014) 201105, https://doi.org/10.1063/1.4879018.
[32] J.-H. Chen, C.-Y. Li, L.-Y. Sun, et al., Polymerization enabled reduction of the electrically induced birefringence change in nematic liquid crystals, Chin. Opt. Lett. 20 (2022) 023201, https://doi.org/10.3788/col202220.023201.
[33] S. Kralj, E.G. Virga, S. Žumer, Biaxial torus around nematic point defects, Phys. Rev. E 60 (2) (1999) 1858–1866, https://doi.org/10.1103/PhysRevE.60.1858.